

# SteganoGAN: Pushing the Limits of Image Steganography

Kevin Alex Zhang  
LIDS, MIT  
kevz@mit.edu

Alfredo Cuesta-Infante  
Univ. Rey Juan Carlos, Spain  
alfredo.cuesta@urjc.es

Kalyan Veeramachaneni  
LIDS, MIT  
kalyanv@mit.edu

## Abstract

Image steganography is a procedure for hiding messages inside pictures. While other techniques such as cryptography aim to prevent adversaries from reading the secret message, steganography aims to hide the presence of the message itself. In this paper, we propose a novel technique based on generative adversarial networks for hiding arbitrary binary data in images. We show that our approach achieves state-of-the-art payloads of 4.4 bits per pixel, evades detection by steganalysis tools, and is effective on images from multiple datasets. To enable fair comparisons, we have released an open source library that is available online at <https://github.com/DAI-Lab/SteganoGAN>.

## 1 Introduction

Steganography has a long and rich history which can be traced back thousands of years to ancient Greece. Ancient steganography techniques relied on unusual properties of physical materials such as invisible ink to hide the presence of a secret message. Modern steganography, on the other hand, relies on the properties of digital files such as images. In a typical image steganography setting, the sender hides (or encodes) a message inside of an image. The receiver, knowing that the image has a message, then uses a decoder to extract it. No one besides the sender and receiver is aware that the image holds a secret message.

Traditional techniques for image steganography can be broadly categorized into three types: (1) methods that take advantage of the file format; (2) methods that operate in the spatial domain [1]; and (3) methods that operate in the frequency domain [2]. The first approach requires an understanding of the file format specification. Most image file formats have special chunks where extra data can be inserted (e.g. text chunks in the PNG format). This technique is simple, but can be easily detected by stripping the unnecessary fields from the image file. The second approach involves replacing the least significant bits (LSB) of the pixels in the image with

data from the message. Algorithms that operate in the spatial domain are primarily differentiated by the way they select pixels for modification. Advanced steganography algorithms such as Highly Undetectable Steganography (HUGO) use high-dimensional statistical models to identify pixels that can be modified with minimal visual distortion [3]. The third approach operates in the frequency domain. This often works by taking a frequency transform of the image and hiding the data in the least significant bits of the coefficients. This type of approach is often more resistant to detection algorithms than techniques that operate in the spatial domain, but is still detectable by automated tools which analyze the distribution of frequency coefficients [2].

In general, these traditional approaches are only effective up to a relative payload of around 0.4 bits per pixel [4]. Beyond that point, they tend to introduce artifacts that can be easily detected by automated steganalysis tools and, in extreme cases, by the human eye. With the advent of deep learning in the past decade, a new class of image steganography approaches are emerging [4–6]. They use neural networks as either a component in a traditional algorithms (e.g. using deep learning to identify spatial locations suitable for embedding data) or as an end-to-end solution, which takes in a cover image and a secret message and combines them into a steganographic image. These attempts at using deep learning for end-to-end image steganography have shown promising results, and have achieved significantly higher embedding rates than the aforementioned techniques. However, they are also more limited than their traditional counterparts, as they often impose special constraints on the size of the cover image [5], make assumptions about the types of data which will be embedded [4], and do not attempt to push the limits of how much information one can hide without being detected [6]. As a result, they fall short of delivering an end-to-end practical solution for the problem. We provide the reader a detailed analysis of these methods in Section 7.

To address these limitations, we propose STEGANOGAN, a novel end-to-end model for image steganography which builds on recent advances in deep learning. We use adver-



Figure 1: A randomly selected cover image (left) and the corresponding steganographic images generated by STEGANOGAN at approximately 1, 2, 3, and 4 bits per pixel.

serial training in which the image steganography task can be formulated as a two-player game between a steganography tool and a steganalysis tool, where both players are neural networks. The two players compete against one another and learn to get better at hiding and detecting messages, respectively. We find that our approach successfully embeds arbitrary data into cover images drawn from a variety of natural scenes and achieves state-of-the-art embedding rates of 4.4 bits per pixel, all while evading standard detection tools.

Figure 1 presents some example images that demonstrate the effectiveness of STEGANOGAN. The left-most figure is the original cover image without any secret messages while the next four figures contain approximately 1, 2, 3, and 4 bits per pixel worth of secret data, respectively, without producing any visible artifacts.

#### Our contributions through this paper are:

- We present a novel deep learning based approach which uses adversarial training to solve the steganography task and achieve a relative payload that is **10x** higher than competing deep learning-based approaches.
- We evaluate our approach for “secrecy”, namely it’s ability to create steganographic images that cannot be detected by automated steganalysis tools. Our experiments demonstrate that our model can hide up to 2 bits per pixel while still ensuring that a state of the art steganalysis tool can only achieve 0.8 auROC.
- We present a new metric for evaluating the capacity of deep learning-based steganography algorithms which can be compared against traditional approaches.
- We are releasing a fully-maintained open-source library called STEGANOGAN<sup>1</sup> including datasets and pre-trained models which can be used to benchmark deep learning based steganography techniques and allow for rapid experimentation.

The rest of the paper is organized as follows. Section 2 briefly describes our motivation for building a better image

steganography system. Section 3 presents STEGANOGAN and describes our model architecture. Section 4 describes our metrics for evaluating model performance. Section 5 contains our experiments for several variants of our model. Section 6 explores the effectiveness of our model at avoiding detection by automated steganalysis tools. Section 7 details related work in the generation of steganographic images, including both traditional and deep learning-based approaches.

## 2 Motivation

There are several reasons to use steganography instead of (or in addition to) cryptography when communicating a secret message between two actors. First, the information contained in a cryptogram is accessible to anyone who has the private key, which poses a challenge in countries where private key disclosure is required by law. Furthermore, the very existence of a cryptogram reveals the presence of a message, which can invite attackers. These problems with plain cryptography exist in security, intelligence services, and a variety of other disciplines [7].

For many of these fields, steganography offers a promising alternative. For example, in medicine, steganography can be used to hide private patient information in images such as X-rays or MRIs [8] as well as biometric data [9]. In the media sphere, steganography can be used to embed copyright data [10] and allow content access control systems to store and distribute digital works over the Internet [11]. In each of these situations, it is important to embed as much information as possible, and for that information to be both *undetectable* and *lossless* to ensure the data can be recovered by the recipient. Most work in the area of steganography, including the methods described in this paper, targets these two goals. We propose a new class of models for image steganography that achieves both these goals.

## 3 SteganoGAN

At a high level, steganography requires just two operations: *encoding* and *decoding*. The *encoding* operation takes a cover

<sup>1</sup><https://github.com/DAI-Lab/SteganoGAN>

image  $C$  of shape  $(3, W, H)$  and a binary message  $b$  and creates a steganographic image  $S$  of shape  $(3, W, H)$ . The *decoding* operation takes the steganographic image  $S$  and recovers the binary message  $b$ . However, we will often impose constraints on the steganographic image such as requiring it to be similar to the cover image and undetectable by steganalysis algorithm.

### 3.1 Overview

In this paper, we propose an approach called STEGANOGAN which parameterizes the two operations above with two convolutional neural networks. In addition, to support adversarial training, we add another convolutional neural network which is used to impose “realism” and “undetectability” constraints on the steganographic image. In this section, we provide an overview of our system and then present the specific architectures.

**Convolutional Neural Networks.** A standard convolutional layer takes an input tensor of size  $(C_{in}, W, H)$  and produces an output tensor of size  $(C_{out}, W, H)$ . It is parameterized by a set of  $C_{out}$  convolutional filters where each filter is of shape  $(C_{in}, k, k)$ ; to generate the output tensor, the convolutional filters are convolved with the input tensor and the outputs from each filter are concatenated together along the channel dimension. By applying non-linear activation functions such as the rectified linear unit (ReLU) or hyperbolic tangent (Tanh) to the output tensor, one can enable a convolutional layer to learn non-linear patterns. By stacking one or more of these convolutional layers on top of one another, we can construct a convolutional neural network (CNN), capable of learning to perform complex tasks simply by finding the set of parameters  $\theta$  which minimize a given loss function.

Since the early outstanding results of AlexNet in 2012 for image recognition [12], Convolutional Neural Networks (CNN) have become an key element in computer vision solutions for detection [13–15], segmentation [16, 17], inpainting [18] and visual tracking [19]. The canonical CNN, as described in [20], is used for supervised tasks with a well-defined loss or cost function and consists of a number of convolutional layers with interleaved pooling layers followed by a fully connected (FC) layer that acts as a classifier or regressor. By rearranging the convolutional layers, pooling layers, and in some cases removing the fully connected layers, we can create new architectures for convolutional neural networks which can be trained to perform more complicated tasks such as image segmentation, in-painting, and generation.

In the context of image steganography, we can use a stack of convolutional layers to implement an encoder which processes an input image of size  $(3, W, H)$  and a data tensor of size  $(D, W, H)$  in order to generate an output image of size  $(3, W, H)$ . Similarly, we can use another stack of convolutional layers to implement a decoder which takes an image of size  $(3, W, H)$  and has a final layer which produces an output

data tensor of size  $(D, W, H)$ . Put together, these two convolutional networks form the backbone of STEGANOGAN; however, in order to improve image quality, we introduce yet another CNN which represents the critic that is used for adversarial training, as discussed in the following section.

**Generative Adversarial Networks.** Generative Adversarial Networks (GANs) were introduced as a way to construct generative models with neural networks [21]. The key idea is that any joint probability distribution function can be transformed into another. Thus, a neural network can be trained to map samples from the standard multivariate normal distribution (MVN) into samples of the distribution over the features of the dataset.

One popular application of GANs is the generation of photo-realistic images. In this setup, a GAN typically consists of a Generator network that maps samples from a MVN into synthetic images. Then, both real and synthetic images are used to train a Detector which aims to detect the synthetic images. Finally, given a trained Detector, the Generator is updated to produce more realistic images that are harder for the Detector to detect.

Training vanilla GANs is an extremely time-consuming and unstable process. Improvements have been proposed for both the network architecture, as in Deep Convolutional GAN [22], Stacked GAN [23] and Progressive Growing GAN [24], as well for the loss functions used to optimize it, as in Energy-based GAN [25], Boundary Equilibrium GAN [26] and the Wasserstein GAN [27].

We focus on the loss function proposed in [27] which uses the Wasserstein distance to measure the difference between the real and the fake distributions. Let  $P_r(x)$  be the real distribution and let  $P_\theta(x)$  be the synthetic distribution parameterized by  $\theta$ , the weights of the neural network. Arjovsk et al. show in [27] that Kullback-Leibler ( $D_{KL}$ ) and Jensen-Shannon ( $D_{JS}$ ) divergences are not appropriate if there are points  $x$  such that  $P_r(x) > 0$  and  $P_\theta(x) = 0$ .

Specifically, if  $P_\theta(x)$  is sufficiently different from  $P_r(x)$ , both  $D_{KL}$  and  $D_{JS}$  are infinite. This is certainly true in the case of a standard convolutional generative adversarial network; due to the high dimensionality of the output space, it is extremely unlikely for a randomly initialized model to produce anything even remotely resembling a natural image and vice versa.

We can avoid this issue by using the Wasserstein distance; details for training Wasserstein GANs are given in Algorithm 1 of [27]. Arjovsk et al. remark that the output of a WGAN is not required to be a probability so the second network can be seen as a Critic that outputs a score rather than a Detector that classifies them. We use the same terminology throughout this paper and use a Critic network to evaluate the quality of our steganographic images.

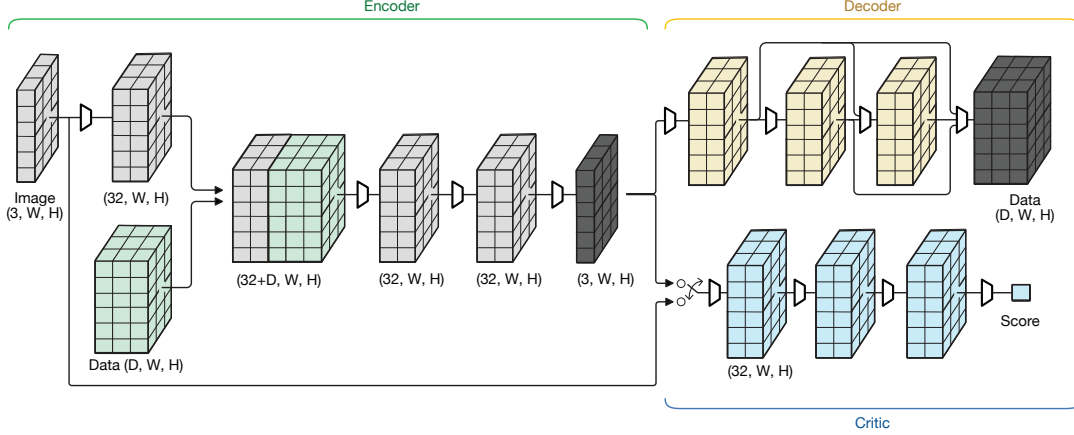


Figure 2: The baseline model architecture with the Encoder, Decoder, and Critic. The Encoder takes in the data tensor and the cover image and outputs a steganographic image. The Decoder receives a steganographic image and outputs the data tensor. The Critic receives an image (either steganographic or cover) and outputs a score. The trapezoids represent convolutional blocks while the arrows represent concatenation operations.

## 3.2 Architecture

In this paper, we propose training a generative adversarial network to hide an arbitrary bit vector in a cover image. We call our method STEGANOGAN and the basic unit of computation in our model is a *convolutional block* which consists of a single convolutional layer with kernel size 3 and stride 1, a leaky rectified linear unit activation function, and a batch normalization layer.

Our proposed architecture, shown in Figure 2, consists of three neural networks: (1) an Encoder that takes a cover image and a data tensor and produces a steganographic image (Section 3.2.1); (2) a Decoder that takes the steganographic image and attempts to recover the data tensor (Section 3.2.2); (3) a Critic that attempts to discriminate between the cover and steganographic images (Section 3.2.3).

### 3.2.1 Encoder

The encoding module takes a cover image of shape  $(3, W, H)$  and a data tensor of shape  $(D, W, H)$  where  $D$  is the number of bits we will attempt to hide in each pixel of the image. We apply a convolutional block to the image to generate a high-dimensional hidden representation of shape  $(T, W, H)$  and concatenate the hidden representation with the data tensor along the color dimension to create a combined tensor of shape  $(3 + T, W, H)$ .

We apply additional convolutional blocks to this combined tensor, which perform further processing before generating the final steganographic output image. In our experiments, we explore three different variants of our architecture which connect these additional convolutional blocks in different ways and examine the impact on model performance.

The final output of each variant is a steganographic image

of shape  $(3, W, H)$  and we minimize the mean squared error loss between the cover image and the steganographic image to encourage the output to resemble the input.

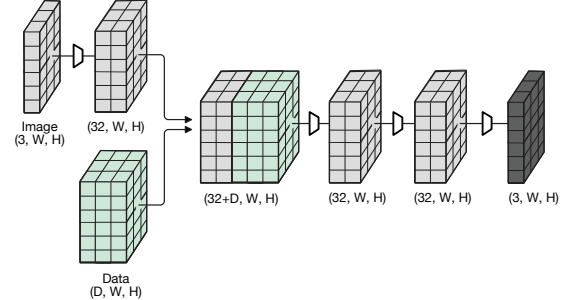


Figure 3: The basic encoder.

**Basic:** In the basic variant of our model, we sequentially apply three convolutional blocks to the combined tensor and generate the steganographic image as shown in Figure 3. This approach is similar to that in [4] as the steganographic image is simply the output of the last convolutional block.

**Residual:** In the residual variant, we apply three convolutional blocks to the combined tensor, as in the basic variant, but instead of generating the steganographic image directly, we generate a residual mask which is added to the original image as shown in Figure 4. The use of residual connections has been shown to improve model stability and convergence [28] so we hypothesize that the use of a residual connection will improve the quality of the steganographic image.

**Dense:** Finally, in the dense variant, we introduce additional connections between the three convolutional blocks so that the feature maps generated by the earlier blocks are concatenated

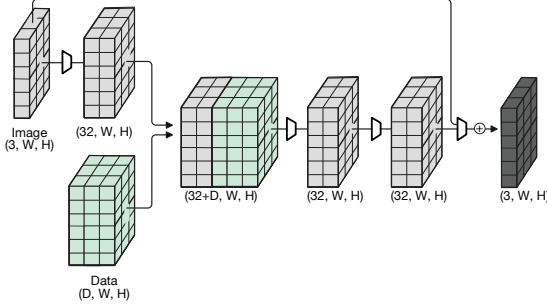


Figure 4: The residual encoder.

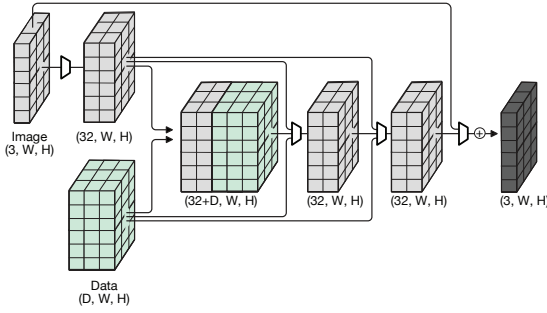


Figure 5: The dense encoder.

to the feature maps generated by later blocks as shown in Figure 5. This connectivity pattern is based on the DenseNet [29] architecture which has been shown to encourage feature reuse and mitigate the vanishing gradient problem. Therefore, we hypothesize that the use of dense connections will improve the embedding rate.

### 3.2.2 Decoder

The decoder module is composed of four convolutional blocks which takes the steganographic image produced by the encoder module and attempts to recover the data tensor. To train this module, we use the binary cross-entropy loss function given by:

$$l_d = -\frac{1}{n} \sum_{i=1}^n (D_i \log(Y_i) + (1 - D_i) \log(1 - Y_i))$$

where  $D$  is the binary target and  $Y$  is the predicted value. Minimizing this loss function is sufficient to train an encoder-decoder pair which is capable of encoding and decoding steganographic images. However, without additional constraints, there is no guarantee that the resulting steganographic image looks natural.

### 3.2.3 Critic

To provide feedback on the performance of our Encoder and generate more realistic images, we introduce an adversarial Critic. The critic module consists of four convolutional blocks followed by a pooling layer which produces a scalar score. We train our critic to minimize the Wasserstein loss function proposed in [27] which attempts to maximize the difference in the score assigned to cover image  $C$  and steganographic image  $S = \text{Encoder}(C, D)$ .

$$l_c = \text{Critic}(C) - \text{Critic}(\text{Encoder}(C, D)).$$

After we have trained our Critic to minimize the score assigned to cover images and maximize the score assigned to steganographic images, we switch to optimizing our Encoder and train it to minimize the score assigned to steganographic images. Intuitively, this procedure forces our Encoder to generate steganographic images which are harder to distinguish from cover images, resulting in more realistic outputs.

---

#### Algorithm 1 Critic

---

- 1: Select a cover image  $C$  of shape  $(3, W, H)$ .
- 2: Generate a data tensor  $D$  of shape  $(D, W, H)$ .
- 3: Create a steganographic image:

$$S = \text{Encoder}(C, D)$$

- 4: Compute the Wasserstein loss:

$$l_c = \text{Critic}(C) - \text{Critic}(S)$$

- 5: Update the critic to minimize the loss.

---

### 3.2.4 Training

During each epoch, we update our model parameters by running Algorithm 1 followed by Algorithm 2 over all cover images in our training set. We use the Adam optimizer with learning rate  $1e-4$ , clip our gradient norm to 0.25, clip the critic weights to  $[-0.1, 0.1]$ , and train for 32 epochs.

During every iteration, we match each training image with a data tensor which consists of a randomly generated sequence of bits sampled from a Bernoulli distribution with parameter  $p = 0.5$ . In addition, we use standard data augmentation procedures including horizontal flipping and random cropping in our pre-processing pipeline.

## 4 Evaluation Metrics

Steganography algorithms are evaluated along three axes: the amount of data that can be hidden in an image, a.k.a *capacity*, the similarity between the cover and steganography image, a.k.a *distortion*, and the ability to avoid detection by



Figure 6: Randomly selected pairs of cover (left) and steganographic (right) images from the MSCOCO dataset which embeds random binary data at the maximum payload of 4.4 bits-per-pixel.

---

**Algorithm 2** Encoder/Decoder

---

- 1: Select a cover image  $C$  of shape  $(3, W, H)$ .
- 2: Generate a data tensor  $D$  of shape  $(D, W, H)$ .
- 3: Create a steganographic image:

$$S = \text{Encoder}(C, D)$$

- 4: Recover the data tensor:

$$Y = \text{Decoder}(S)$$

- 5: Compute the decoder loss:

$$l_d = -\frac{1}{n} \sum_{i=1}^n (D_i \log(Y_i) + (1 - D_i) \log(1 - Y_i))$$

- 6: Compute the mean squared loss for Encoder:

$$l_e = \frac{1}{n} \sum_{i=1}^n (\text{Encoder}(C, D)_i - C_i)^2$$

- 7: Compute the Wasserstein loss:

$$l_c = \text{Critic}(S)$$

- 8: Update the encoder and decoder to minimize the total loss  $l_d + l_e + l_c$ .

---

steganalysis tools, a.k.a *secrecy*. This section describes some metrics for evaluating the performance of our model along these axes.

**Reed Solomon Bits Per Pixel:** Measuring the effective number of bits that can be conveyed per pixel is non-trivial in our setup since the ability to recover a hidden bit is heavily dependent on the model and the cover image, as well as the message itself.

To model this situation, suppose that a given model incorrectly decodes a bit with probability  $p$ . It is tempting to just multiply the number of bits in the data tensor by the accuracy  $1 - p$  and report that value as the relative payload. Unfortunately, that value is actually meaningless – it allows you to estimate the number of bits that have been correctly decoded, but does not provide a mechanism for recovering from errors or even identifying which bits are correct.

Therefore, to get an accurate estimate of the relative payload of our technique, we turn to Reed-Solomon codes. Reed-Solomon error-correcting codes are a subset of linear block codes which offer the following guarantee: Given a message of length  $k$ , the code can generate a message of length  $n$  where  $n \geq k$  such that it can recover from  $\frac{n-k}{2}$  errors [30]. This implies that given a steganography algorithm which, on average, returns an incorrect bit with probability  $p$ , we would want the number of incorrect bits to be less than or equal to the number of bits we can correct:

$$pn \leq \frac{n-k}{2} \quad (1)$$

The ratio  $k/n$  represents the average number of bits of "real" data we can transmit for each bit of "message" data; then, from (1), it follows that the ratio is less than or equal to  $1 - 2p$ . As a result, we can measure the relative payload of our steganographic technique by multiplying the number of bits we attempt to hide in each pixel by the ratio to obtain the "real" number of bits that is transmitted and recovered.

We refer to this metric as Reed-Solomon bits-per-pixel (RS-BPP), and note that it can be directly compared against traditional steganographic techniques since it represents the average number of bits that can be reliably transmitted in an image divided by the size of the image.

**Peak Signal to Noise Ratio:** In addition to measuring the relative payload, we also need to measure the quality of the steganographic image. One widely-used metric for measuring image quality is the peak signal-to-noise ratio (PSNR). This metric was originally designed to measure image distortions and has been shown to be correlated with mean opinion scores produced by human experts [31].

Given two images  $X$  and  $Y$  of size  $(M, N)$  and a scaling factor  $\text{sc}$  which represents the maximum possible difference in the numerical representation of each pixel<sup>2</sup>, the PSNR is defined as a function of the mean squared error (MSE):

$$\text{MSE} = \frac{1}{M \cdot N} \sum_i^M \sum_j^N (X_{i,j} - Y_{i,j})^2,$$

$$\text{PSNR} = 20 \cdot \log_{10}(\text{sc}) - 10 \cdot \log_{10}(\text{MSE}).$$

Although PSNR is widely used to evaluate the distortion produced by steganography algorithms, [32] suggests that it may not be ideal for comparisons across different types of steganography algorithms. Therefore, we introduce another metric to help us evaluate image quality: the structural similarity index.

**Structural Similarity Index:** In our experiments, we also report the structural similarity index (SSIM) between the cover image and the steganographic image. SSIM is widely used in the broadcast industry to measure image and video quality [31]. Given two images  $X$  and  $Y$ , the SSIM can be computed using the means,  $\mu_X$  and  $\mu_Y$ , variances,  $\sigma_X^2$  and  $\sigma_Y^2$ , and covariance  $\sigma_{XY}^2$  of the images as shown below:

$$\text{SSIM} = \frac{(2\mu_X\mu_Y + k_1R)(2\sigma_{XY} + k_2R)}{(\mu_X^2 + \mu_Y^2 + k_1R)(\sigma_X^2 + \sigma_Y^2 + k_2R)}$$

The default configuration for SSIM uses  $k_1 = 0.01$  and  $k_2 = 0.03$  and returns values in the range  $[-1.0, 1.0]$  where 1.0 indicates the images are identical.

<sup>2</sup>For example, if the images are represented as floating point numbers in  $[-1.0, 1.0]$ , then  $\text{sc} = 2.0$  since the maximum difference between two pixels is achieved when one is 1.0 and the other is  $-1.0$ .

	# Train	# Test	Description
Div2K	800	100	High resolution images of diverse scenes.
MSCOCO	118,287	40,670	Low resolution images of common objects.

Table 1: A high-level description of the two datasets used in our experiments.

## 5 Results and Analysis

We use the Div2k [33] and MSCOCO [34] datasets, described in Table 1, to train and evaluate our model. We experiment with each of the three model variants discussed in Section 3 and train them with 6 different data depths  $D \in \{1, 2, \dots, 6\}$ . The data depth  $D$  represents the "target" bits per pixel so the randomly generated data tensor has shape  $D \times W \times H$ .

We use the default train/test split proposed by the creators of the Div2K and MSCOCO data sets in our experiments, and we report the average RS-BPP, PSNR, and SSIM on the test set in Table 2. Our models are trained on GeForce GTX 1080 GPUs. The wall clock time per epoch is approximately 10 minutes for Div2K and 2 hours for MSCOCO.

After training our model, we compute the expected accuracy on a held-out test set and adjust it using the Reed-Solomon coding scheme discussed in Section 4 to produce our bits-per-pixel metric, shown in Table 2 under RS-BPP. We publicly released the pre-trained models for all the experiments shown in this table on AWS S3<sup>3</sup>.

Figure 6 shows pairs of images picked at random from the MSCOCO dataset. The cover image is shown on the left and the steganographic image containing approximately 4.4bpp is shown on the right. We notice almost no visual artifacts or distortion. In Figure 7, we compare our model's output to that of a naive least-significant-bit steganography algorithm and show evidence that our model is responsive to image content.

The results from our experiments are shown in Table 2 – each of the metrics is computed on a held-out test set of images that is not shown to the model during training. Note that there is an unavoidable tradeoff between the relative payload and the image quality measures; assuming we are already on the Pareto frontier, an increased relative payload would inevitably result in a decreased similarity.

We immediately observe that all variants of our model perform better on the MSCOCO dataset than the Div2K dataset. This can be attributed to differences in the type of content photographed in the two datasets. Images from the Div2K dataset tend to contain open scenery, while images from the MSCOCO dataset tend to be more cluttered and contain multiple objects, providing more surfaces and textures for our model to successfully embed data.

<sup>3</sup><http://steganogan.s3.amazonaws.com/index.html>

Dataset	Depth	Accuracy			RS-BPP			PSNR			SSIM		
		Basic	Residual	Dense	Basic	Residual	Dense	Basic	Residual	Dense	Basic	Residual	Dense
Div2K	1	0.954	0.993	0.996	0.908	0.987	0.992	24.522	41.675	41.597	0.7	0.957	0.954
	2	0.912	0.981	0.989	1.651	1.924	1.956	24.624	38.245	39.615	0.674	0.898	0.921
	3	0.82	0.92	0.938	1.92	2.521	2.627	25.032	36.665	36.518	0.689	0.853	0.852
	4	0.748	0.815	0.816	1.983	2.519	2.53	24.452	37.86	37.488	0.687	0.875	0.881
	5	0.686	0.739	0.75	1.862	2.391	2.5	24.901	39.45	38.652	0.696	0.902	0.895
	6	0.67	0.693	0.703	2.041	2.318	2.44	24.722	39.531	38.943	0.696	0.908	0.9
MSCOCO	1	0.982	0.995	0.994	0.964	0.99	0.989	31.214	41.714	42.09	0.868	0.977	0.979
	2	0.971	0.991	0.991	1.884	1.966	1.965	31.556	39.003	39.082	0.855	0.959	0.952
	3	0.944	0.974	0.978	2.667	2.849	2.869	30.158	37.383	36.927	0.826	0.928	0.921
	4	0.874	0.95	0.951	2.993	3.602	3.61	31.121	36.977	36.943	0.827	0.915	0.919
	5	0.842	0.899	0.924	3.426	3.992	4.24	29.731	36.686	36.613	0.803	0.899	0.908
	6	0.778	0.838	0.866	3.344	4.065	4.403	31.415	36.745	36.334	0.838	0.894	0.881

Table 2: The relative payload and image quality metrics for each dataset and model variant. The Dense model variant offers the best performance across all metrics in almost all experiments.



Figure 7: A randomly selected pair of cover (left) and steganographic (right) images and the differences between them. The top row shows the output from a simple least-significant-bit steganography algorithm [35] while the bottom row shows the output from STEGANOGAN with 4.4 bpp. Note that STEGANOGAN is able to adapt to the objects in the image.

In addition, we note that our dense variant shows the best performance on both relative payload and image quality, followed closely by the residual variant which shows comparable image quality but a lower relative payload. The basic variant offers the worst performance across all metrics, achieving relative payloads and image quality scores that are 15-25% lower than the dense variant.

Finally, we remark that despite the increased relative payload, the image similarity as measured by the average peak signal to noise ratio between the cover image and the steganographic images produced by the Dense models are comparable to that presented in [6].

## 6 Detecting Steganographic Images

Steganography techniques are also typically evaluated by their ability to evade detection by steganalysis tools. In this section, we experiment with two open source steganalysis algorithms and measure our model’s ability to generate undetectable steganographic images.

### 6.1 Statistical Steganalysis

We use a popular open-source steganalysis tool called StegExpose [36] which combines several existing steganalysis techniques including Sample Pairs [37], RS Analysis [38], Chi Squared Attack [39], and Primary Sets [40]. To measure the effectiveness of our method at evading detection by these techniques, we randomly select 1,000 cover images from the test set, generating the corresponding steganographic images using our Dense architecture with data depth 6, and examine the results using StegExpose.

The receiver operating characteristic curve for our Dense model is shown in Figure 8 and we note that the StegExpose tool is only slightly more effective than random guessing with an area under the ROC curve of 0.59, even for payloads of up to 4.4 bits per pixel. This shows that our model can successfully evade standard steganalysis tools, meeting the minimum requirement for being a viable steganography algorithm.

### 6.2 Neural Steganalysis

Recent studies have shown promising results in detecting steganographic images using deep learning based approaches [41]. Therefore, we proceed to examine whether our model can evade deep learning-based steganalysis tools. We use the model proposed by Ye et al., 2017 in [41] for steganalysis, with a slight modification to enable support of color images, and train it to detect steganographic images generated by STEGANOGAN.

In a typical scenario, the party that is attempting to detect steganographic images has access to the algorithm used

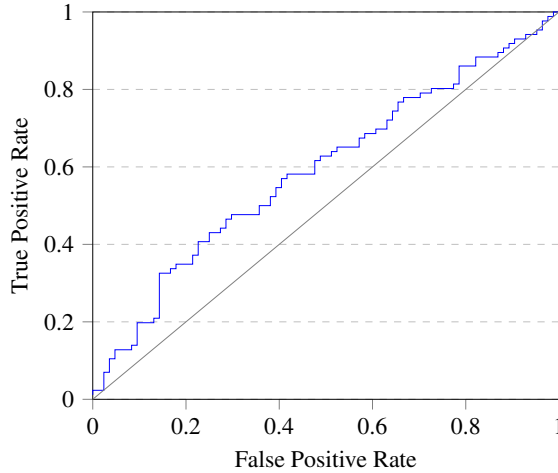


Figure 8: The receiver operating characteristic (ROC) curve produced by the StegExpose library for a set of 1000 steganographic images generated using the Dense architecture with a data depth of 6. The StegExpose library includes multiple steganalysis tools including SamplePairs [37], RSAnalysis [38], ChiSquaredAttack [39], and PrimarySets [40]. The tool achieves an auROC of 0.59.

to create them - in our case, an instance of STEGANOGAN which is parameterized by the pretrained model weights but not the exact model. Using the Dense architecture from Section 3.2.1 and the MSCOCO dataset, we attempt to replicate this scenario with the following experimental setup:

1. We train  $N$  instances of the Dense STEGANOGAN architecture with different random seeds.
2. For each of these trained models, we generate a set of 1,000 steganographic images.
3. Holding out the images generated by the  $N$ th model as a test set, we train the steganalysis model proposed in [41] on increasing subsets of the remaining images  $\{1\}, \{1, 2\}, \{1, 2, 3\}, \dots, \{1, 2, 3, \dots, N-1\}$ .
4. We repeat each experiment 3 times and report the average area under the receiver operating curve in Figure 9.

This emulates a realistic setting - the party creating the automatic detection model will not have access to the specific STEGANOGAN model in use, but may have access to the software used to train the models. Therefore, we pose the following question: If the external party does not know the specific model weights but does know the algorithm for generating models, can they detect steganographic images generated by STEGANOGAN?

Figure 9 shows the performance of our detector for various relative payloads and training set sizes. First, we note that

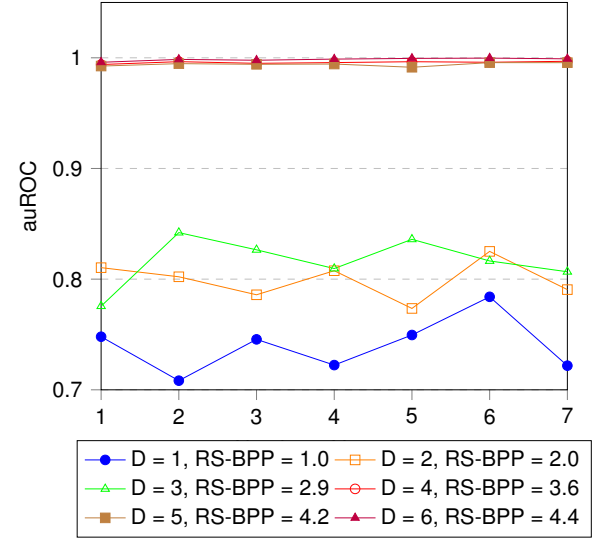


Figure 9: This plot shows the performance of the steganography detector on a held-out test set. The x-axis indicates the number of different STEGANOGAN instances that were used, while the y-axis indicates the area under the ROC curve.

the detector performance, as measured by the area under the receiver operating characteristic (auROC), increases as we increase the number of bits-per-pixel encoded in the image. In addition, we highlight the fact that contrary to our expectations, there is no clear trend in the area under the ROC curve as we increase the number of STEGANOGAN models used for training. This suggests that the external party will have a difficult time building a model which can detect steganographic images generated by STEGANOGAN without knowing the exact model parameters.

Finally, we compare the detection error for images generated by STEGANOGAN against those reported by [41] on images generated by three state-of-the-art steganography algorithms: WOW [42], S-UNIWARD [43], and HILL [44]. Note that these techniques are evaluated on different dataset and as such, the results are only approximate estimates of the actual relative payload achievable on a particular dataset. For a fixed detection error rate of 20%, we find that WOW is able to encode up to 0.3 bpp, S-UNIWARD is able to encode up to 0.4 bpp, HILL is able to encode up to 0.5 bpp, and STEGANOGAN is able to encode up to 2.0 bpp.

## 7 Related Work

In this section, we describe a few traditional approaches to image steganography and then discuss recent approaches developed using deep learning.

## 7.1 Traditional Approaches

A standard algorithm for image steganography is "Highly Undetectable steGO" (HUGO), a cost function-based algorithm which uses handcrafted features to measure the distortion introduced by modifying the pixel value at a particular location in the image. Given a set of  $N$  bits to be embedded, HUGO uses the distortion function to identify the top  $N$  pixels that can be modified while minimizing the total distortion across the image [3].

Another approach is the JSteg algorithm, which is designed specifically for JPEG images. JPEG compression works by transforming the image into the frequency domain using the discrete cosine transform and removing high-frequency components, resulting in a smaller image file size. JSteg uses the same transformation into the frequency domain, but modifies the least significant bits of the frequency coefficients [2].

The effectiveness of image steganography algorithms is frequently measured in bits per pixel (bpp). Traditional steganography algorithms such as HUGO are designed to embed arbitrary data into cover images — with no assumptions about the distribution of the data — and report their relative payload in bpp, based on the total number of bits hidden in the image divided by the number of pixels in the image.

## 7.2 Deep Learning for Steganography

Deep learning for image steganography has recently been explored in several studies, all showing promising results. These existing proposals range from training neural networks to integrate with and improve upon traditional steganography techniques [45] to complete end-to-end convolutional neural networks which use adversarial training to generate convincing steganographic images [5, 6].

**Hiding images vs. arbitrary data:** The first set of deep learning approaches to steganography were [4, 46]. Both [4] and [46] focus solely on taking a *secret image* and embedding it into a *cover image*. Because this task is fundamentally different from that of embedding arbitrary data, it is difficult to compare these results to those achieved by traditional steganography algorithms in terms of the relative payload.

Natural images such as those used in [4] and [46] exhibit strong spatial correlations, and convolutional neural networks trained to hide images in images would take advantage of this property. Therefore, a model that is trained in such a manner cannot be applied to arbitrary data. Even if we were to coerce arbitrary binary data (e.g. a string) into an image by reinterpreting the bits as pixels, the resulting image would not resemble natural images due to the lack of local spatial correlations, and could not be successfully embedded.

**Adversarial training:** The next set of approaches for image steganography are [5, 6] which make use of adversarial training techniques. The key differences between these approaches and our approach are the loss functions used to train

the model, the architecture of the model, and how data is presented to the network.

The method proposed by [5] can only operate on images of a fixed size. Their approach involves flattening the image into a vector, concatenating a bit vector filled with data to the image vector, and applying feedforward, reshaping, and convolutional layers. They use the mean squared error to optimize the encoder, the cross entropy loss for the discriminator, and the mean squared error for the decoder. They report that image quality suffers greatly when attempting to increase the number of bits beyond 0.4 bits per pixel.

The method proposed by [6] uses the same loss functions as [5] but makes changes to the model architecture. Specifically, they “*replicate the message spatially, and concatenate this message volume to the encoder’s intermediary representation.*” For example, in order to hide  $k$  bits in an  $N \times N$  image, they would create a tensor of shape  $(k, N, N)$  where the data vector is replicated at each spatial location.

This design allows [6] to handle arbitrary sized images simply by creating more copies of the data vector. However, this design cannot effectively scale to higher relative payloads. For example, to achieve a relative payload of 1 bit per pixel in a typical image of size  $360 \times 480$ , they would need to manipulate a data tensor of size  $(172800, 360, 480)$ . Therefore, due to the excessive memory requirements, this model architecture cannot effectively scale to handle large relative payloads.

In contrast, our model architecture does not repeat the message spatially; instead, we distribute the message across the spatial dimensions of our message. For example, in order to achieve a relative payload of 2 bits per pixel, we would place the first two bits at the top left corner of the image, the next two bits one pixel over, and so on. This dramatically reduces the size of the data tensor as well as the number of parameters in our model.

Of course, this means that not every bit of data will be exposed to every pixel in the image. For example, the bits located in the top left corner may not interact at all with the pixels in the bottom right corner, making it more difficult to hide data. However, in our experiments, we find that our model is able to compensate due to large effective convolutional windows. This means that our architecture is able to scale to both large images and large payloads.

Finally, we use a different set of loss functions which have been empirically shown to improve model performance in related computer vision literature. We use the mean squared error loss for the encoder, the cross entropy loss for the decoder, and the Wasserstein loss function for the detector [27].

**Inaccurate bpp estimates:** One of the challenges of using deep learning-based approaches to perform image steganography is dealing with the presence of uncertainty. Traditional steganography algorithms avoid this issue, as they typically guarantee perfect recovery of the data as long as the image has not been modified.

	Hayes et al, 2017 [5]	Zhu et al, 2018 [6]	STEGANOGAN
<b>Data Constraints</b>	Arbitrary binary data	Arbitrary binary data	Arbitrary binary data
<b>Image Constraints</b>	$32 \times 32$	Any size	Any size
<b>Loss Functions:</b>			
Encoder	MSE	MSE	MSE
Decoder	MSE	MSE	Cross entropy
Critic	Cross entropy	Cross entropy	Wasserstein
<b>Data Tensor</b>	Flattened bit vector.	Repeated bit vector.	Expanded bit tensor.
<b>Architecture</b>	Flatten, append, convolve.	Convolve, append, convolve.	Convolve, append, convolve.
<b>Best Bits-Per-Pixel</b>	0.4	0.2	4.4
<b>Bits-Per-Pixel Type</b>	Unadjusted BPP	Unadjusted BPP	Reed-Solomon BPP
<b>Notes</b>	<i>“... we found after 0.4bpp, image quality suffered and it was no longer possible to balance realistic image creation capable of fooling Eve, and convergence of message decoding”</i>	<i>“... our model closely matches the baselines on BPP (0.203 vs 0.200).”</i>	

Table 3: A comparison of several recently developed deep learning-based steganography algorithms which use convolutional neural networks and adversarial training.

This is not true in the deep learning setup since the decoding accuracy is heavily dependent on the cover image. Both [5] and [6] have avoided answering this question by only considering models which achieve near-perfect decoding accuracy. This approach produces results which are correct and can be compared to traditional algorithms, but also results in overly conservative estimates of the relative payload, since any models that do not achieve perfect accuracy are unusable.

On the other hand, in [46], the authors define their *decoding rate* and *capacity* (in bits-per-pixel) as below, where  $S$  is the secret image,  $R$  is the recovered image and both are of size  $(N, M)$ :

$$\text{Rate} = 1 - \frac{\sum_{i=1}^N \sum_{j=1}^M |S_{i,j} - R_{i,j}|}{N \cdot M},$$

$$\text{Bits Per Pixel} = \text{Rate} \times 8 \times 3.$$

The authors explain that their metric computes the "percent" of an image that is recovered and multiplies it by the number of bits required to represent the uncompressed RGB bitmap to estimate the total bits per pixel. However, the "percent" measure presented in [46] is not the percent of bits recovered successfully but rather one minus the mean absolute deviation which, despite being interpretable as a "percent," does not actually correspond to the "percent" of bits which are successfully recovered.

Furthermore, even after addressing the above issue and using a revised "percent" measure, this metric only indicates the number of bits that are correctly recovered, not the number of bits that can actually be transmitted. For example, using this metric, a decoder that returns random bits with equal probability would achieve a relative payload of 0.5 bits per pixel, since – assuming the input data follows a similar distribution – approximately half the bits would be "correct" by random chance.

As a result, we assert that this metric does not correspond to the standard interpretation of relative payload and bits per pixel as the size of the largest message which can be encoded and decoded with perfect accuracy divided by the size of the cover image.

**Summary:** In summary, we find that previous studies on applying deep learning to image steganography suffer from three major limitations: (a) they impose constraints on the types of and size of the data that can be embedded; (b) they restrict the size and shape of the cover image; and (c) they cannot be directly benchmarked against traditional steganography algorithms.

To address these issues, we designed (1) a new architecture for end-to-end image steganography which supports arbitrary data, and (2) use adversarial training to improve performance of the deep learning method on the task (2) a new metric for measuring the relative payload in a manner which allows the

results to be directly compared against those from traditional steganography algorithms.

## 8 Conclusion

In this paper, we introduced a flexible new approach to image steganography which supports different-sized cover images and arbitrary binary data. Furthermore, we proposed a new metric for evaluating the performance of deep-learning based steganographic systems so that they can be directly compared against traditional steganography algorithms. We experiment with three variants of the STEGANOGAN architecture and demonstrate that our model achieves higher relative payloads than existing approaches while still evading detection.

## Acknowledgements

The authors would like to thank Plamen Valentinov Kolev and Carles Sala for their help with software support and developer operations as well as Lei Xu for the helpful discussions and feedback. Finally, the authors would like to thank Accenture for their generous support and funding which made this research possible.

## References

- [1] M. Hussain, A. W. A. Wahab, Y. I. B. Idris, A. T. Ho, and K.-H. Jung, “Image steganography in spatial domain: A survey,” *Signal Processing: Image Communication*, vol. 65, pp. 46 – 66, 2018.
- [2] B. Li, J. He, J. Huang, and Y. Shi, “A survey on image steganography and steganalysis,” *Journal of Information Hiding and Multimedia Signal Processing*, 2011.
- [3] T. Pevný, T. Filler, and P. Bas, “Using high-dimensional image models to perform highly undetectable steganography,” in *Information Hiding*, 2010.
- [4] S. Baluja, “Hiding images in plain sight: Deep steganography,” in *Advances in Neural Information Processing Systems 30* (I. Guyon, U. V. Luxburg, S. Bengio, H. Wallach, R. Fergus, S. Vishwanathan, and R. Garnett, eds.), pp. 2069–2079, Curran Associates, Inc., 2017.
- [5] J. Hayes and G. Danezis, “Generating steganographic images via adversarial training,” in *NIPS*, 2017.
- [6] J. Zhu, R. Kaplan, J. Johnson, and L. Fei-Fei, “HiDDeN: Hiding data with deep networks,” *CoRR*, vol. abs/1807.09937, 2018.
- [7] M. Conway, “Code wars: Steganography, signals intelligence, and terrorism,” *Knowledge, Technology & Policy*, vol. 16, pp. 45–62, Jun 2003.
- [8] Y. Srinivasan, B. Nutter, S. Mitra, B. Phillips, and D. Ferris, “Secure transmission of medical records using high capacity steganography,” in *Proc. of the 17th IEEE Symposium on Computer-Based Medical Systems*, pp. 122–127, June 2004.
- [9] M. Douglas, K. Bailey, M. Leeney, and K. Curran, “An overview of steganography techniques applied to the protection of biometric data,” *Multimedia Tools and Applications*, vol. 77, pp. 17333–17373, Jul 2018.
- [10] S. U. Maheswari and D. J. Hemanth, “Frequency domain qr code based image steganography using fresnelet transform,” *AEU - International Journal of Electronics and Communications*, vol. 69, no. 2, pp. 539 – 544, 2015.
- [11] E. Kawaguchi, M. Maeta, H. Noda, and K. Nozaki, “A model of digital contents access control system using steganographic information hiding scheme,” in *Proc. of the 18th Conf. on Information Modelling and Knowledge Bases*, pp. 50–61, 2007.
- [12] A. Krizhevsky, I. Sutskever, and G. E. Hinton, “Imagenet classification with deep convolutional neural networks,” *Commun. of the ACM*, vol. 60, pp. 84–90, May 2017.
- [13] S. Ren, K. He, R. B. Girshick, and J. Sun, “Faster R-CNN: Towards Real-Time Object Detection with Region Proposal Networks,” in *NIPS*, pp. 91–99, 2015.
- [14] J. Redmon, S. Divvala, R. Girshick, and A. Farhadi, “You only look once: Unified, real-time object detection,” in *The IEEE Conf. on Computer Vision and Pattern Recognition (CVPR)*, June 2016.
- [15] W. Liu, D. Anguelov, D. Erhan, C. Szegedy, S. Reed, C.-Y. Fu, and A. C. Berg, “SSD: Single Shot MultiBox Detector,” in *Computer Vision – ECCV*, pp. 21–37, Springer International Publishing, 2016.
- [16] V. Badrinarayanan, A. Kendall, and R. Cipolla, “Segnet: A deep convolutional encoder-decoder architecture for image segmentation,” *IEEE Trans. on Pattern Analysis and Machine Intelligence*, vol. 39, pp. 2481–2495, Dec 2017.
- [17] W. Li, O. H. Jafari, and C. Rother, “Deep object co-segmentation,” *CoRR*, vol. abs/1804.06423, 2018.
- [18] C. Yang, X. Lu, Z. Lin, E. Shechtman, O. Wang, and H. Li, “High-resolution image inpainting using multi-scale neural patch synthesis,” in *IEEE Conf. on Computer Vision and Pattern Recognition (CVPR)*, July 2017.
- [19] L. Leal-Taixé, C. Canton-Ferrer, and K. Schindler, “Learning by tracking: Siamese cnn for robust target association,” in *IEEE Conf. on Computer Vision and Pattern Recognition Workshops (CVPRW)*, pp. 418–425, June 2016.
- [20] Y. Lecun, L. Bottou, Y. Bengio, and P. Haffner, “Gradient-based learning applied to document recognition,” *Proceedings of the IEEE*, vol. 86, pp. 2278–2324, Nov 1998.
- [21] I. J. Goodfellow, J. Pouget-Abadie, M. Mirza, B. Xu, D. Warde-Farley, S. Ozair, A. C. Courville, and Y. Bengio, “Generative adversarial nets,” in *NIPS*, pp. 2672–2680, 2014.
- [22] A. Radford, L. Metz, and S. Chintala, “Unsupervised representation learning with deep convolutional generative adversarial networks,” in *Int. Conf. on Learning Representations (ICLR)*, 2016.
- [23] X. Huang, Y. Li, O. Poursaeed, J. Hopcroft, and S. Belongie, “Stacked generative adversarial networks,” in *IEEE Conf. on Computer Vision and Pattern Recognition (CVPR)*, pp. 1866–1875, July 2017.

[24] T. Karras, T. Aila, S. Laine, and J. Lehtinen, “Progressive growing of gans for improved quality, stability, and variation,” in *Int. Conf. on Learning Representations (ICLR)*, 2018.

[25] J. J. Zhao, M. Mathieu, and Y. LeCun, “Energy-based generative adversarial network,” in *Int. Conf. on Learning Representations (ICLR)*, 2017.

[26] D. Berthelot, T. Schumm, and L. Metz, “BEGAN: boundary equilibrium generative adversarial networks,” *CoRR*, vol. abs/1703.10717, 2017.

[27] M. Arjovsky, S. Chintala, and L. Bottou, “Wasserstein generative adversarial networks,” in *Proc. of the 34th Int. Conf. on Machine Learning, ICML*, pp. 214–223, 2017.

[28] K. He, X. Zhang, S. Ren, and J. Sun, “Deep residual learning for image recognition,” *IEEE Conf. on Computer Vision and Pattern Recognition (CVPR)*, pp. 770–778, 2016.

[29] G. Huang, Z. Liu, L. van der Maaten, and K. Q. Weinberger, “Densely connected convolutional networks,” *IEEE Conf. on Computer Vision and Pattern Recognition (CVPR)*, pp. 2261–2269, 2017.

[30] I. S. Reed and G. Solomon, “Polynomial Codes Over Certain Finite Fields,” *Journal of the Society for Industrial and Applied Mathematics*, vol. 8, no. 2, pp. 300–304, 1960.

[31] Z. Wang, A. C. Bovik, H. R. Sheikh, and E. P. Simoncelli, “Image quality assessment: from error visibility to structural similarity,” *IEEE Trans. on Image Processing*, vol. 13, pp. 600–612, April 2004.

[32] A. Almohammad and G. Ghinea, “Stego image quality and the reliability of psnr,” in *2010 2nd International Conference on Image Processing Theory, Tools and Applications*, pp. 215–220, July 2010.

[33] E. Agustsson and R. Timofte, “NTIRE 2017 challenge on single image super-resolution: Dataset and study,” in *The IEEE Conf. on Computer Vision and Pattern Recognition (CVPR) Workshops*, July 2017.

[34] T. Lin, M. Maire, S. J. Belongie, L. D. Bourdev, R. B. Girshick, J. Hays, P. Perona, D. Ramanan, P. Dollár, and C. L. Zitnick, “Microsoft COCO: common objects in context,” *CoRR*, vol. abs/1405.0312, 2014.

[35] N. Johnson and S. C. Katzenbeisser, “A survey of steganographic techniques,” 01 1999.

[36] B. Boehm, “StegExpose - A tool for detecting LSB steganography,” *CoRR*, vol. abs/1410.6656, 2014.

[37] S. Dumitrescu, X. Wu, and Z. Wang, “Detection of LSB steganography via sample pair analysis,” in *Information Hiding*, pp. 355–372, 2003.

[38] J. Fridrich, M. Goljan, and R. Du, “Reliable detection of lsb steganography in color and grayscale images,” in *Proc. of the 2001 Workshop on Multimedia and Security: New Challenges, MM’01, Sec ’01*, pp. 27–30, ACM, 2001.

[39] A. Westfeld and A. Pfitzmann, “Attacks on steganographic systems,” in *Information Hiding*, pp. 61–76, 2000.

[40] S. Dumitrescu, X. Wu, and N. Memon, “On steganalysis of random lsb embedding in continuous-tone images,” vol. 3, pp. 641 – 644 vol.3, 07 2002.

[41] J. Ye, J. Ni, and Y. Yi, “Deep learning hierarchical representations for image steganalysis,” *IEEE Trans. on Information Forensics and Security*, vol. 12, pp. 2545–2557, Nov 2017.

[42] V. Holub and J. Fridrich, “Designing steganographic distortion using directional filters,” 12 2012.

[43] V. Holub, J. Fridrich, and T. Denemark, “Universal distortion function for steganography in an arbitrary domain,” *EURASIP Journal on Information Security*, vol. 2014, p. 1, Jan 2014.

[44] B. Li, M. Wang, J. Huang, and X. Li, “A new cost function for spatial image steganography,” in *2014 IEEE Int. Conf. on Image Processing (ICIP)*, pp. 4206–4210, Oct 2014.

[45] W. Tang, S. Tan, B. Li, and J. Huang, “Automatic steganographic distortion learning using a generative adversarial network,” *IEEE Signal Processing Letters*, vol. 24, pp. 1547–1551, Oct 2017.

[46] P. Wu, Y. Yang, and X. Li, “Stegnet: Mega image steganography capacity with deep convolutional network,” *Future Internet*, vol. 10, p. 54, 06 2018.